Appl. Phys. A (2014) 116:1033–1039
DOI 10.1007/s00339-014-8335-1

Applied Physics A
Materials Science & Processing

A novel strongly correlated electronic thin-film laser energy/power meter based on anisotropic Seebeck effect

G.-Y. Zhang · H. Zhang · S.-L. Tan · P.-X. Zhang · T.-Y. Tseng · H.-U. Habermeier · C.-T. Lin · P. Singjai

Received: 29 November 2013 / Accepted: 17 February 2014 / Published online: 6 March 2014

Abstract Strongly correlated electronic (SCE) materials including high-temperature superconducting cuprate and colossal magnetoresistance manganite thin films demonstrate tremendous anisotropic Seebeck effect which makes them very promising for developing high-performance laser detectors. In this work, laser-induced thermoelectric voltage (LITV) signals with nanosecond response time have been measured in SCE $La_{1-x}Pb_xMnO_3$ thin films based on anisotropic Seebeck effect at room temperature. The magnitude of the LITV signals increases linearly with laser energy/power density in a wide range of laser wavelengths from ultraviolet, visible to infrared based on which a novel SCE thin-film laser energy/power meter has been developed.

G.-Y. Zhang · P. Singjai (✉)
Department of Physics and Materials Science, Faculty of Science, Chiang Mai University, Chiang Mai 50200, Thailand
e-mail: singjai@chiangmai.ac.th

G.-Y. Zhang · T.-Y. Tseng
Department of Electronics Engineering and Institute of Electronics, National Chiao Tung University, Hsinchu 300, Taiwan

G.-Y. Zhang (✉)
Hefei National Laboratory for Physical Science at Microscal, University of Science and Technology of China, Hefei 230026, People's Republic of China
e-mail: zhanggy@ustc.edu.cn

H. Zhang · S.-L. Tan · P.-X. Zhang
Institute of Advanced Materials for Photoelectronics, Kunming University of Science and Technology, Kunming 650051, People's Republic of China

H.-U. Habermeier · C.-T. Lin
Max Planck Institute for Solid State Research, Heisenbergstrasse 1, 70569 Stuttgart, Germany

1 Introduction

Strongly correlated electronic (SCE) materials have attracted much attention in recent years owing to their abundant and exotic electrical, magnetic, optical, thermal, acoustic, mechanical and chemical properties resulting from the strong interactions between charge, spin, orbital and lattice degrees of freedom, which are important not only for developing new theories but also for exploring new applications [1–3]. At present, the research on SCE materials has become a hot frontier of modern science since the discoveries of high-temperature superconductivity (HTS) in cuprates and colossal magnetoresistance (CMR) effect in manganites, where a small change of magnetic field causes a great variation of resistance due to a metal–insulator transition in the vicinity of the ferromagnetic Curie point [4–11].

Apart from the profound and dramatic phenomena such as HTS and CMR, SCE materials also display diversified phase diagrams which reveal the complex electrical and magnetic structures of these materials [2]. In general, the phase diagram of hole (electron)- doped HTS cuprates shows that at low doping levels, electron repulsion causes an exchange interaction resulting in an antiferromagnetic ordering, and at higher doping levels a superconducting region is created with the pseudo gap state above it [12]. For the CMR materials with the formula $Re_{1-x}A_xMnO_3$ (Re: a trivalent rare earth element, and A: a divalent element), the phase diagrams show that their electrical and magnetic properties strongly depend on two parameters: the band filling (or the doping level x) and the conduction bandwidth (or electron hopping interaction) [13]. The typical CMR materials such as $La_{1-x}Ca_xMnO_3$ (LCMO), $La_{1-x}Sr_xMnO_3$ (LSMO) and $La_{1-x}Pb_xMnO_3$ (LPMO) are especially interesting because they show long-range

ordering of the Mn^{3+} ($t_{2g}^3 e_g^1$) and Mn^{4+} ($t_{2g}^3 e_g^0$) ions which is linked to the antiferromagnetic spin ordering, the long-range ordering of the Mn^{3+} (e_g) orbitals and the associated lattice distortions [14]. Furthermore, it is known that LCMO is an intermediate-bandwidth CMR material. At $x = 0$ and 1, it is A- and G-type ordering antiferromagnetic, respectively; in the region $0.2 \leq x \leq 0.5$, the ground state is ferromagnetic metallic; while for $x > 0.5$, the ground state becomes insulating and charge-ordered antiferromagnetic [15]. LSMO is a large-bandwidth CMR material and a canonical double-exchange (DE) system. It has maximal Curie temperature (T_c) (380 K for $x \approx 1/3$) in CMR systems and grows easily in large single crystals at $x \leq 0.4$. In addition, it has relatively simple phase diagram: it is antiferromagnetic insulating for $x < 0.10$ and ferromagnetic insulating for $0.10 < x < 0.165$, above which it is ferromagnetic metallic [16]. Besides LSMO, LPMO is another high-T_c CMR material whose T_c is in the range of 315–361 K for $x = 0.1$–0.5 and is almost constant (about 360 K) for $x \geq 0.3$ [17, 18]. The advantages such as high-T_c above room temperature (RT), ferromagnetic metallic ground state at RT, and large magnetoresistance at RT make LPMO an ideal material for developing RT and high-temperature magnetic devices [17–25].

At the beginning of the 1990s, laser-induced thermoelectric voltage (LITV) effect was discovered in HTS thin films such as $YBa_2Cu_3O_{7-x}$ (YBCO) and $Bi_2Sr_2CaCu_2O_8$ (BSCCO) which opened up new areas of research to developing high-performance laser detectors based on SCE thin films [26–28]. Photoelectric effect, pyroelectricity and piezoelectricity are usually employed to analyze light-induced voltage phenomena; however, none of them could satisfactorily explain the laser-induced voltage effect in YBCO thin films. At last, the effect observed in YBCO thin films was proved to be anisotropic Seebeck effect, or LITV effect [26–29]. It is known that for HTS cuprate single crystals, the Seebeck coefficient of the conductive CuO_2 layer is different from that along c-axis, i.e., the Seebeck coefficient of the crystals is a tensor rather than a scalar [30, 31]. When a HTS thin film grows on a vicinal cut single-crystal substrate, its c-axis inclines an angle to the normal of its surface; and the sequence of the conducting CuO_2 layers and the less-conducting intermediate layers forms an atomic layer thermopile (ALT) that consists of some millions of atomic scale thermocouples [27]. When a laser pulse irradiates on the thin-film surface, the up layer of the surface absorbs the energy and its temperature increases which erects a temperature gradient in the inner of the film, and due to the ALT effect a voltage generates along the film surface—that is the microscopic mechanism of the LITV effect [32]. Soon after, LITV effect was found in LCMO thin films [33, 34]. It is unexpected that large LITV signals can be generated in LCMO thin films because LCMO has a quasi-cubic structure which leads to small anisotropy, and therefore no obvious voltage signals should be observed. However, the magnitude of the induced voltage signals in LCMO thin films strongly depends on the doping level revealing that it is the electrical structure rather than crystal structure that plays a key role, i.e., it is the long-range cooperative Jahn–Teller distortions caused by the Mn^{3+} ions resulting in the large anisotropy [34]. Interestingly, it is observed that CMR materials doped with other divalent ions such as LSMO and LPMO thin films also show large LITV effect as described in Reference [35] and this work, which not only confirms this theory but also provides a new method to explore CMR mechanism. SCE thin-film laser detectors based on ALT effect have super advantages. It has been reported that LITV signals of about 400 ps have been measured in ~10-nm-thick YBCO thin films at RT [36]; LITV signals as high as 250 V have been recorded in YBCO thin films grown with a large tilt angle $\alpha \sim 10$–$20°$ [32]; and YBCO thin films can respond to radiation over a very wide wavelength range from ultraviolet to millimeter wave [32]. In addition, more importantly, based on LITV effect high-performance laser energy/power meter can be designed. We have developed kinds of laser energy/power meters based on YBCO, LCMO and LSMO thin films, which all show great advantages over other conventional detectors, such as fast (nanosecond order) response, spectrally broad (from infrared through visible to ultraviolet) response and spectrally flat response [35, 37, 38]. In this work, we develop a novel LPMO thin-film laser energy/power meter based on LITV effect, which not only enriches the study on SCE mechanism, but also opens a new door to design high-performance laser energy/power meter with high-T_c.

2 Theory

The LITV signal in a SCE thin film is given by the formula [39]:

$$U(t) = \frac{\alpha_0 El \sin(2\alpha)}{4d\rho c_0 \sqrt{\pi D t}} (S_{ab} - S_c) \left(e^{-\frac{\delta^2}{4Dt}} - e^{-\frac{d^2}{4Dt}} \right), \quad (1)$$

Where α_0 is the laser absorption coefficient of film, E is the laser energy density per pulse, l is the illuminated length of film, α is the tilted angle, $S_{ab} - S_c$ is the Seebeck coefficient anisotropy, ρ is the mass density, c_0 is the specific heat, δ is the laser penetrating depth into the thin-film material, D is the thermal diffusion constant and d is the film thickness.

The peak value of LITV signal U_p is given by

$$U_p = A_p E, \tag{2}$$

where A_p is the sensitivity and

$$A_p = \frac{\alpha_0 l \sin(2\alpha)}{4\sqrt{\pi} d \rho c_0} |(S_{ab} - S_c) f(\delta, d)|, \tag{3}$$

where $f(\delta, d)$ is the function about δ and d. Based on the linear relationship $U_p = A_p E$, a peak voltage-type laser energy meter can be designed. Because the response time is proportional to $1/D$, in order to obtain fast response SCE material with large D can be selected. Furthermore, Eq. (3) shows that A_p is independent of D, therefore, the response speed can be raised by increasing D without changing the sensitivity.

3 Experimental

LPMO thin films were grown on $LaAlO_3$ (LAO) single-crystal substrates by pulsed laser deposition technique. A polycrystalline target of nominal composition LPMO was synthesized by a coprecipitation method. The laser beam from a pulsed KrF excimer laser of wavelength 248 nm, pulse width 20 ns was focused onto the rotating target. An optimized laser fluency of 1.6 J/cm^2 and repetition rate of 5 Hz was utilized. The depositions were carried out in the oxygen pressure of 0.4 mbar and at a substrate temperature of 780 °C. After the deposition, the samples were annealed in situ at 530 °C for 1 h in the oxygen pressure of 1 bar, and then the films were cooled to RT in about 30 min. The structure characterization was made by X-ray diffraction. Two methods were used to test the prototype LPMO laser energy/power meter. One method is for pulsed laser detection in which the LITV signals are recorded by a digital oscilloscope, as shown in Fig. 1a. The other one is for continuous-wave (CW) laser detection, in which a lock-in amplifier is used to obtain high signal-to-noise ratio, as shown in Fig. 1b.

4 Results and discussion

X-ray diffraction indicates all the LPMO thin films deposited on LAO substrates are single-phase and (001)-oriented since besides (00l) peaks, the LPMO thin films show no peaks originating from impurities [40].

LITV experiments were performed at RT, and a 360-nm-thick $La_{2/3}Pb_{1/3}MnO_3$ thin film grown on a 15° tilted LAO substrate was used for laser irradiation. Figure 2 shows a typical LITV signal induced by the

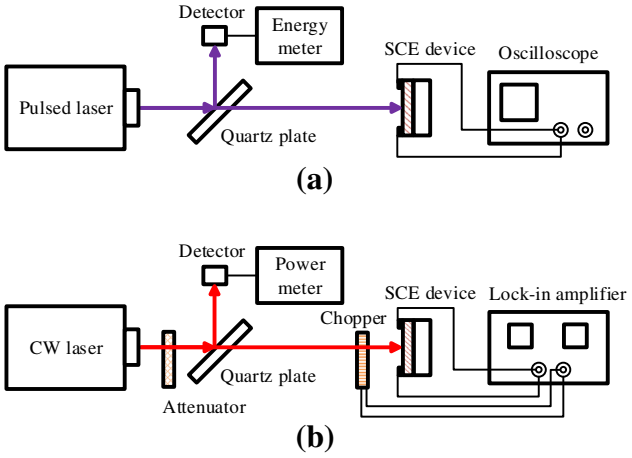

Fig. 1 Two schematic diagrams of the two methods used to measure LITV signals in a SCE device induced by **a** pulsed and **b** CW lasers, respectively

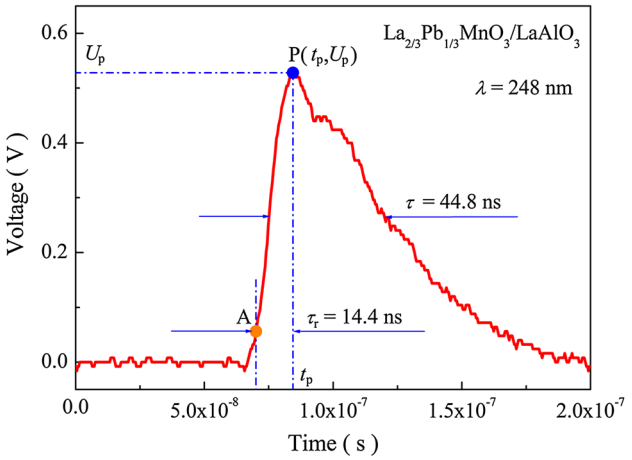

Fig. 2 A typical LITV signal in $La_{2/3}Pb_{1/3}MnO_3$ thin film induced by the pulsed KrF excimer laser with $\lambda = 248$ nm. U_p is the peak voltage. $\tau_r = 14.4$ ns and $\tau = 44.8$ ns

pulsed KrF excimer laser. A LITV signal is characterized by its response time and peak value. To analyze the response time we define two parameters: the rise time τ_r (the time taken from 10 to 100 % of the signal peak) and the signal width τ (FWHM—the full width at half-maximum of the signal). It can be seen the $La_{2/3}Pb_{1/3}MnO_3$ thin film has nanosecond response time: its τ_r and τ are 14.4 and 44.8 ns, respectively. It has been reported T_c of $La_{2/3}Pb_{1/3}MnO_3$ can be as high as 361 K [41], and thus below T_c and at RT its ground state is ferromagnetic metallic, which results in high electrical conductivity. According to Wiedemann–Franz law ($\kappa/\sigma = LT$, where κ, σ, L, and T are thermal conductivity, electrical conductivity, Lorenz number, and temperature, respectively), at the same temperature κ is proportional to σ, i.e., D is proportional to σ. Therefore, the existence of ferromagnetic metallic state

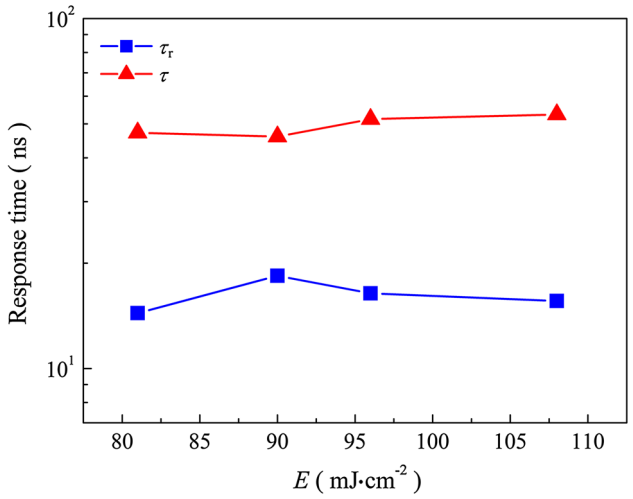

Fig. 3 Laser energy density dependence of response time

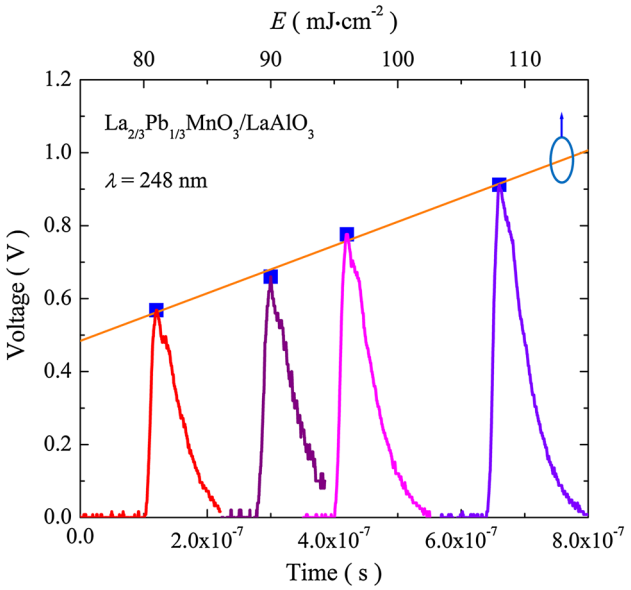

Fig. 4 The linear relationship between U_p and the laser energy density for $\lambda = 248$ nm

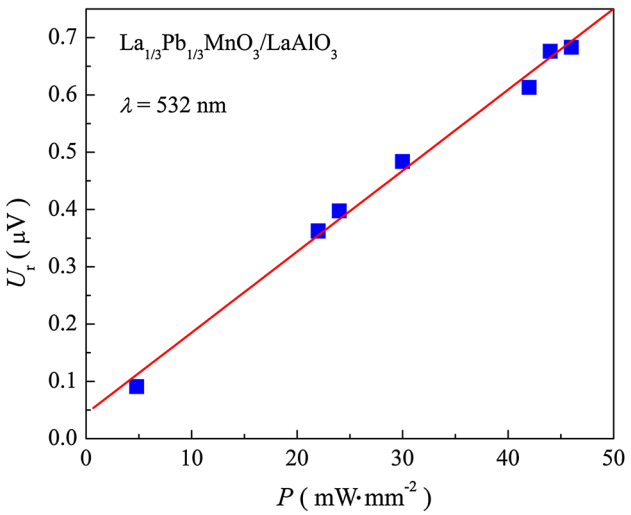

Fig. 5 The linear relationship between U_r and the laser power density for $\lambda = 532$ nm

makes the $La_{2/3}Pb_{1/3}MnO_3$ thin film have large σ and D, and as a result ns-order response is achieved. On the other hand, for LPMO with different doping levels x, σ increases with T_c at the same temperature [42], i.e., high-T_c will lead to fast response. $La_{2/3}Pb_{1/3}MnO_3$ has the highest T_c among LPMO systems, which makes it greater potential for obtaining faster response than LPMO with other doping levels. Similar properties have been observed in LSMO: it is ferromagnetic metallic at RT due to its high-T_c, and at RT its τ_r and τ are $\leq$23 and $<$39 ns, respectively [35]. These results indicate that high-T_c SCE materials are unique materials for designing fast detectors working at RT. Figure 3 shows laser energy density dependence of response time. It is observed that as the laser energy density increases the response time nearly keeps unchanged, which indicates the energy density of the pulsed KrF excimer laser has a small influence on D, demonstrating the $La_{2/3}Pb_{1/3}MnO_3$ thin film has high chemical and thermal stability. Figure 4 shows the linear relationship between U_p and E, which not only confirms Eq. (2), but also indicates A_p has high stability under high-energy laser irradiation. Besides the pulsed KrF excimer laser, three CW lasers ($\lambda = 532$, 632.8, and 808 nm) were also employed to test the $La_{2/3}Pb_{1/3}MnO_3$ thin-film detector. A linear relationship $U_r = A_rP$ has been measured at each wavelength, where U_r, A_r and P are the readout voltage of the lock-in amplifier, the sensitivity and the laser power density, respectively, as shown in Figs. 5, 6, 7. The wavelength dependence of the sensitivity is shown in Fig. 8. It is seen the sensitivity has spectrally broad response which ranges from ultraviolet, visible, to infrared. Furthermore, it has spectrally flat response. The slight variation of sensitivity with wavelength is attributed to quantum effect and α_0. The band gap of the $La_{2/3}Pb_{1/3}MnO_3$ thin film is 1.2 eV [43, 44], which is smaller than the photon energy of the 808 nm (1.53 eV), 632.8 nm (1.96 eV), 532 nm (2.33 eV) and 248 nm (5.00 eV) lasers. The carriers generated by each laser enhance the film conductivity, and thus increases the sensitivity. However, high-energy photons can generate lots of hot carriers which cannot be absorbed effectively by the electrodes [45, 46], and the energy loss of the laser caused by the hot carriers will decrease the sensitivity. As a result, as the laser wavelength decreases the sensitivity increases firstly in the wavelength range of 808–632.8 nm and then decreases in the wavelength range of 632.8–248 nm. Besides photoconductive effect, α_0 also causes some variation because it varies with laser

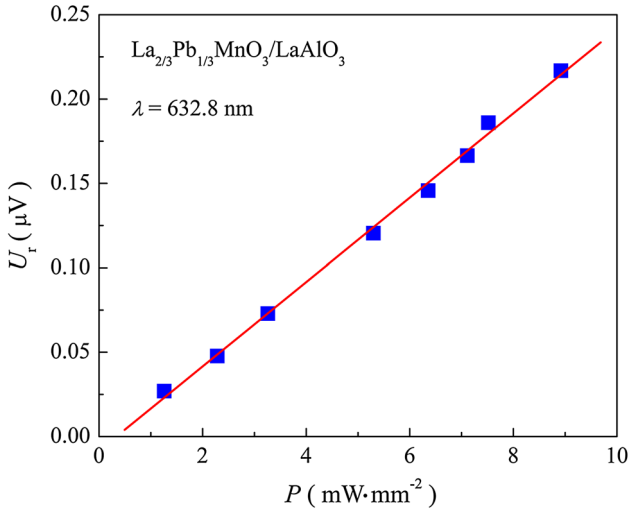

Fig. 6 The linear relationship between U_r and the laser power density for $\lambda = 632.8$ nm

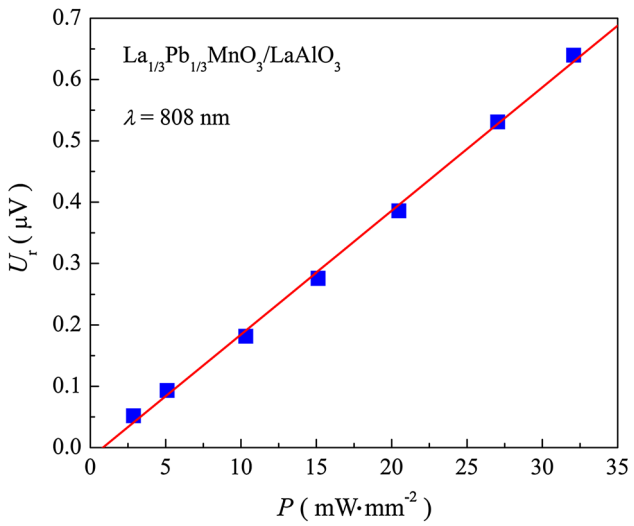

Fig. 7 The linear relationship between U_r and the laser power density for $\lambda = 808$ nm

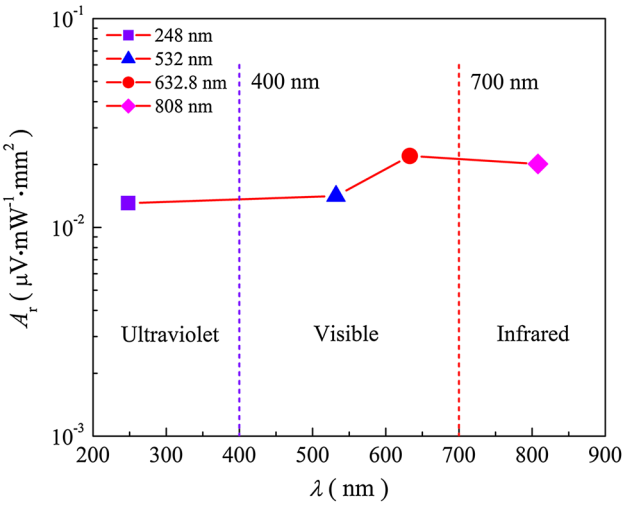

Fig. 8 Wavelength dependence of the sensitivity of the $La_{2/3}Pb_{1/3}MnO_3$ thin-film device at RT

wavelength which prevents the thin film from absorbing the incident laser constantly. To obtain uniform light absorption, an efficient absorbing layer or some nanostructures can be fabricated on the surface of the thin film [47–49].

Anisotropic Seebeck effect is characterized by Seebeck anisotropy coefficient $\Delta S = S_{ab} - S_c$, and $|\Delta S|$ can be calculated using $|\Delta S| = \kappa U_p \sqrt{\tau_0 \tau_d \pi}/[\alpha_0 El \sin(2\alpha)]$, where τ_0 is the laser pulse width and τ_d is the time constant which can be obtained by fitting the decay curve of the LITV signal [50, 51]. Using $U_p = 0.528$ V, $\kappa = 3.23$ W m^{-1} K^{-1}, $\tau_0 = 20$ ns, $\tau_d = 39.4$ ns, $\alpha_0 = 0.82$, $E = 87$ mJ cm^{-2}, $l = 1$ mm, and $\alpha = 15^\circ$, $|\Delta S|$ of the $La_{2/3}Pb_{1/3}MnO_3$ thin film is calculated to be 0.24 μV K^{-1}. Table 1 lists the typical values of $|\Delta S|$, τ_r, τ and T_c for various thermoelectric materials and devices. For Seebeck effect $|\Delta S| = |S_A - S_B|$, where S_A and S_B are the Seebeck coefficients of materials A and B, respectively. It can be seen based on Seebeck and anisotropic Seebeck effects different kinds of thermoelectric detectors have been developed. T_c of CMR materials is higher than that of HTS materials. Among CMR materials, T_c ($|\Delta S|$) of $La_{2/3}Pb_{1/3}MnO_3$ is lower than that of $La_{2/3}Sr_{1/3}MnO_3$ ($La_{2/3}Ca_{1/3}MnO_3$), but it is higher than that of $La_{2/3}Ca_{1/3}MnO_3$ ($La_{2/3}Sr_{1/3}MnO_3$). Relatively high $|\Delta S|$ and T_c and ns-order response make $La_{2/3}Pb_{1/3}MnO_3$ a promising material for developing novel detectors. Furthermore, $|\Delta S|$ of an Al/n-Si superlattice detector is 1.5 mV K^{-1}, which is the highest value among the thermoelectric devices. Crystalline Bi has the second highest $|\Delta S|$ (52 μV K^{-1}), however, its response time is slow (100 μs–1 ms). In contrast, p-Si/SiGe and copper/constantan superlattice detectors have relatively high $|\Delta S|$ and ns-order response. Compared with the detectors based on anisotropic Seebeck effect, although the microthermocouple and microthermopile detectors based on Seebeck effect have relatively high $|\Delta S|$, they suffer slow response time (10^1–10^2 μs). Furthermore, Eq. (3) shows A_p is proportional to l, thus the sensitivity of SCE detectors can be increased by simply increasing the thin film length. In contrast, based on Seebeck effect, to achieve high sensitivity individual microthermocouples can be connected in series to form a microthermopile detector. Figures 5, 6, 7 show U_r is below 1 μV, indicating the $La_{2/3}Pb_{1/3}MnO_3$ detector has a low sensitivity for detecting CW lasers, which results from the small values of l and $|\Delta S|$, 1 mm and 0.24 μV K^{-1}, respectively. To increase the sensitivity, the experiments to increase l and to optimize the parameters such as doping ion, doping level and substrate to increase $|\Delta S|$ will be carried out in the near future. In summary, although so many different kinds of laser detectors have been developed based on Seebeck and

Table 1 Typical values of $|\Delta S|$, τ_r, τ, and T_c for various thermoelectric materials and devices

Thermoelectric effect	Thermoelectric material/device			$\lvert\Delta S\rvert$ ($\mu V\ K^{-1}$)	τ_r (ns)	τ (ns)	T_c (K)	References
Anisotropic Seebeck effect	SCE system	CMR	LaPbMnO	2.4×10^{-1}	1.44×10^{1}	4.48×10^{1}	361	This work
			LaSrMnO	1.4×10^{-1}	2.10×10^{1}	3.65×10^{1}	380	[35, 52]
			LaCaMnO	3.62	2.73×10^{1}	3.80×10^{1}	263.5	[38, 53]
		HTS	YBaCuO	1.0×10^{1}	2.5×10^{-1}	4.0×10^{-1}	92	[36]
			BiSrCaCuO	3.0×10^{1}	1.05×10^{1}	4.70×10^{1}	85	[28]
			TlBaCaCuO	4.7×10^{-2}	1.64×10^{1}	3.03×10^{1}	108	[54, 55]
	Crystal	Metal	Bi	5.2×10^{1}	–	1×10^{5}–1×10^{6}	–	[56]
	Superlattice	Metal/alloy	Copper/constantan	3.54×10^{1}	1.19×10^{2}	5.04×10^{2}	–	[57]
		Alloy/alloy	Chromel/constantan	5	–	1×10^{5}	–	[56, 58]
		Semiconductor/semiconductor	p-Si/SiGe	2.0×10^{1}	2.39×10^{1}	3.0×10^{1}	–	[51]
		Metal/semiconductor	Al/n-Si	1.5×10^{3}	–	–	–	[58]
Seebeck effect	Microthermocouple	Metal/metal	Au/Pd	4.5	7.58×10^{5}	8.53×10^{5}	–	[59]
	Microthermopile	Metal/alloy	Copper/constantan	3.0×10^{1}	3.92×10^{4}	–	–	[60]

anisotropic Seebeck effects, SCE detectors are more attractive because of their exotic and abundant physical and chemical properties.

Research on SCE systems enriches our understanding of solid state physics and provides a new route toward multifunctional devices. In this work, a novel SCE LPMO thin-film laser energy/power meter is developed not only offering more material choice for designing high-performance laser detectors and laser energy/power meters but also opening a new direction for constructing novel high-T_c SCE devices with combined optical, electrical, thermal and magnetic properties which work at RT and high temperatures above RT. Furthermore, the SCE system-based laser detectors and laser energy/power meters demonstrate super advantages over other conventional devices and technologies. First, the SCE devices have high thermal and chemical stability which makes their response time and sensitivity very stable under high-power laser irradiation. The SCE devices can measure high-power ($>10^7$ W) laser directly; however, common semiconducting detectors usually need attenuators to prevent them from being destroyed when measuring high-power laser. Second, the SCE devices have large dynamic range. The linear relationship between the magnitude of the LITV signals and the laser energy/power density exists in a very wide laser power range of 10 orders of magnitude (10^{-3}–10^7 W). Third, the SCE devices have fast (ps- to ns-order) response and spectrally broad (almost unlimited) and flat response at the same time. In contrast, although semiconducting detectors have fast response they suffer from a narrow band of wavelengths due to quantum effect. In contrast, although thermal sensors such as bolometers have spectrally broad response, their response speed is usually slow (typically ms order) since a thermal equilibrium process is required. Fourth, the SCE devices can respond to both direct current (DC) and alternating current (AC) signals and perform in situ real-time measurements, whereas pyroelectric detectors can only respond to AC signals, and a signal modulation process is needed when they measure DC signals [35, 61, 62]. Fifth, the SCE devices are energy-saving devices since they are self-powered due to thermoelectric effect. In contrast, bolometers and thermistors need bias in order to sense the resistance changes. At last, the SCE systems provide wider material choice for developing kinds of high-performance multifunctional devices.

5 Conclusions

A novel SCE LPMO thin-film laser energy/power meter has been developed based on anisotropic Seebeck effect. It demonstrates great advantages over other conventional devices such as ns-order response and spectrally broad (from ultraviolet, visible to infrared) and flat response, high thermal and chemical stability, response to both DC and AC signals, in situ real-time measurement at RT, large dynamic range and energy savings, and can be a useful replacement for the commercial pyroelectric laser detectors and laser energy meters. In conclusion, taking the high-T_c LPMO

device as an example, we have revealed the great potential of SCE systems for developing next-generation high-performance laser detectors and laser energy/powers based on anisotropic Seebeck effect and novel multifunctional high-T_c devices working at RT and high temperatures above RT.

Acknowledgments This work was supported by China Postdoctoral Science Foundation (Grant No. 20070410218), the Postdoctoral Foundation of University of Science and Technology of China, the National Natural Science Foundation of China (Grant No. 10274026), and the Natural Science Foundation of Yunnan Province of China (Grant No. 1999E0003Z).

References

1. G.Y. Zhang, P.X. Zhang, H.-U. Habermeier, in *Handbook of Interferometers; Research, Technology and Applications*, ed. by D. Halsey, W. Raynor (Nova Science, New York, 2009)
2. E. Dagotto, Science **309**, 257 (2005)
3. Y. Tokura, N. Nagaosa, Science **288**, 462 (2000)
4. A. Shekhter, B.J. Ramshaw, R.X. Liang, W.N. Hardy, D.A. Bonn, F.F. Balakirev, R.D. McDonald, J.B. Betts, S.C. Riggs, A. Migliori, Nature **498**, 75 (2013)
5. H.-C. Jiang, M.S. Block, R.V. Mishmash, J.R. Garrison, D.N. Sheng, O.I. Motrunich, M.P.A. Fisher, Nature **493**, 39 (2013)
6. C.L. Smallwood, J.P. Hinton, C. Jozwiak, W.T. Zhang, J.D. Koralek, H. Eisaki, D.H. Lee, J. Orenstein, A. Lanzara, Science **336**, 1137 (2012)
7. K.J. Lai, M. Nakamura, W. Kundhikanjana, M. Kawasaki, Y. Tokura, M.A. Kelly, Z.X. Shen, Science **329**, 190 (2010)
8. K.H. Ahn, T. Lookman, A.R. Bishop, Nature **428**, 401 (2004)
9. C.H. Ahn, J.M. Triscone, J. Mannhart, Nature **424**, 1015 (2003)
10. S. Jin, T.H. Tiefel, M. McCormack, R.A. Fastnacht, R. Ramesh, L.H. Chen, Science **264**, 413 (1994)
11. M. Eichberger, H. Schäfer, M. Krumova, M. Beyer, J. Demsar, H. Berger, G. Moriena, G. Sciaini, R.J.D. Miller, Nature **468**, 799 (2010)
12. N. Nagaosa, Science **275**, 1078 (1997)
13. Y. Tokura, Y. Tomioka, J. Magn. Magn. Mater. **200**, 1 (1999)
14. C.N.R. Rao, J. Phys. Chem. B **104**, 5877 (2000)
15. A.J. Millis, Nature **392**, 147 (1998)
16. L.P. Gor'kov, V.Z. Kresin, Phys. Rep. **400**, 149 (2004)
17. N. Chau, H.N. Nhat, N.H. Luong, D.L. Minh, N.D. Tho, N.N. Chau, Phys. B **327**, 270 (2003)
18. G.H. Jonker, J.H. Van Santen, Physica **16**, 337 (1950)
19. S. Sundar Manoharan, N.Y. Vasanthacharya, M.S. Hegde, K.M. Satyalakshmi, V. Prasad, S.V. Subramanyam, J. Appl. Phys. **76**, 3923 (1994)
20. E. Vladimirova, V. Vassiliev, A. Nossov, J. Mater. Sci. **36**, 1481 (2001)
21. A.M. Niraimathi, M. Hofmann, Phys. B **276–278**, 722 (2000)
22. R. Mahendiran, R. Mahesh, A.K. Raychaudhuri, C.N.R. Rao, J. Phys. D **28**, 1743 (1995)
23. E. Burzo, I. Balasz, I.G. Deac, M. Neumann, R. Tetean, Phys. B **403**, 1601 (2008)
24. T.L. Phan, S.G. Min, M.H. Phan, N.D. Ha, N. Chau, S.C. Yu, Phys. Stat. Sol. (b) **244**, 1109 (2007)
25. A.V. Kartashev, E.A. Mikhaleva, M.V. Gorev, E.V. Bogdanov, A.V. Cherepakhin, K.A. Sablina, N.V. Mikhashonok, I.N. Flerov, N.V. Volkov, J. Appl. Phys. **113**, 073901 (2013)
26. C.L. Chang, A. Kleinhammes, W.G. Moulton, L.R. Testardi, Phys. Rev. B **41**, 11564 (1990)
27. H. Lengfellner, G. Kremb, A. Schnellbogl, J. Betz, K.F. Renk, W. Prettl, Appl. Phys. Lett. **60**, 501 (1992)
28. W.M. Huber, S.T. Li, A. Ritzer, D. Bäuerle, H. Lengfellner, W. Prettl, Appl. Phys. A **64**, 487 (1997)
29. H.-U. Habermeier, N. Jisrawi, G. Jäger-Waldau, Appl. Surf. Sci. **96–98**, 689 (1996)
30. S. Zeuner, W. Prettl, H. Lengfellner, Appl. Phys. Lett. **66**, 1833 (1995)
31. P.X. Zhang, G.Y. Zhang, C.T. Lin, H.-U. Habermeier, Egypt. J. Sol. **27**, 1 (2004)
32. K.F. Renk, J. Betz, S. Zeuner, H. Lengfellner, W. Prettl, Phys. C **235–240**, 37 (1994)
33. H.-U. Habermeier, X.H. Li, P.X. Zhang, B. Leibold, Solid State Commun. **110**, 473 (1999)
34. X.H. Li, H.-U. Habermeier, P.X. Zhang, J. Magn. Magn. Mater. **211**, 232 (2000)
35. G.Y. Zhang, H.R. Zheng, X.Y. Zhang, D.L. Gao, P.X. Zhang, H.U. Habermeier, Appl. Phys. B **108**, 649 (2012)
36. Th Zahner, R. Stierstorfer, S. Reindl, T. Schauer, A. Penzkofer, H. Lengfellner, Phys. C **313**, 37 (1999)
37. P.X. Zhang, X.M. Wen, M.M. Gu, G.Y. Zhang, Chin. J. Lasers **29**, 205 (2002)
38. G.Y. Zhang, H.R. Zheng, W.H. Huang, X.Y. Zhang, D.L. Gao, H. Zhang, P.X. Zhang, T.Y. Tseng, H.U. Habermeier, C.T. Lin, H.H. Cheng, Appl. Phys. A **113**, 347 (2013)
39. P.X. Zhang, W.K. Lee, G.Y. Zhang, Appl. Phys. Lett. **81**, 4026 (2002)
40. S.L. Tan, H. Zhang, W.D. Cui, Y. Yuan, P.X. Zhang, Acta Phys. Sin. **55**, 4226 (2006)
41. N. Mtiraoui, A. Dhahri, M. Oumezine, J. Dhahri, E. Dhahri, J. Magn. Magn. Mater. **323**, 22 (2011)
42. C.W. Searle, S.T. Wang, Can. J. Phys. **48**, 2023 (1970)
43. J.-H. Park, E. Vescovo, H.-J. Kim, C. Kwon, R. Ramesh, T. Venkatesan, Nature **392**, 794 (1998)
44. J.-H. Park, C.T. Chen, S.-W. Cheong, W. Bao, G. Meigs, V. Chakarian, Y.U. Idzerda, Phys. Rev. Lett. **76**, 4215 (1996)
45. A.J. Nozik, Phys. E **14**, 115 (2002)
46. G. Conibeer, Mater. Today **10**, 42 (2007)
47. W. Lang, K. Kühl, H. Sandmaier, Sens. Actuators A **34**, 243 (1992)
48. S.B. Rim, S. Zhao, S.R. Scully, M.D. McGehee, P. Peumans, Appl. Phys. Lett. **91**, 243501 (2007)
49. J. Zhao, A. Wang, P. Altermatt, M.A. Green, Appl. Phys. Lett. **66**, 3636 (1995)
50. J.T. Hu, H.S. Li, J. Zhu, G.Y. Zhang, P.X. Zhang, Chin. J. Lasers **36**, 1214 (2009)
51. X.F. Zhou, Z.M. Jiang, J.H. Lin, X.D. Tang, Q.M. Chen, H. Zhang, P.X. Zhang, J. Phys. D **42**, 225303 (2009)
52. X. Liu, Y.Z. Yan, Q.M. Chen, H. Zhang, X.P. Yin, Appl. Phys. A (2013). doi:10.1007/s00339-013-8013-8
53. J. Ma, H. Zhang, Q.M. Chen, X. Liu, J. Appl. Phys. **114**, 043708 (2013)
54. D.G. Naugle, A.B. Kaiser, in *Thallium-based high-temperature superconductors*, ed. by A.M. Hermann, J.V. Yakhmi (Marcel Dekker, New York, 1994), p. 559
55. H.Y. Zhang, H.S. Huang, B. Tang, L.F. Zhang, Z.S. Zhang, M.L. Liu, Phys. C **282–287**, 1275 (1997)
56. K. Fischer, C. Stoiber, A. Kyarad, H. Lengfellner, Appl. Phys. A **78**, 323 (2004)
57. Th Zahner, R. Förg, H. Lengfellner, Appl. Phys. Lett. **73**, 1364 (1998)
58. A. Kyarad, H. Lengfellner, Appl. Phys. Lett. **85**, 5613 (2004)
59. B. Serio, H. Gualous, J.P. Prenel, Sens. Actuators A **84**, 303 (2000)
60. T.A.S. Srinivas, P.J. Timans, R.J. Butcher, H. Ahmed, Appl. Phys. Lett. **59**, 1529 (1991)
61. H. Lengfellner, S. Zeuner, W. Prettl, K.F. Renk, Europhys. Lett. **25**, 375 (1994)
62. H.S. Kwok, J.P. Zheng, Phys. Rev. B **46**, 3692 (1992)